

Atom chips with two-dimensional electron gases: near surface trapping and ultracold-atom microscopy of quantum electronic systems

G. Sinuco-León, B. Kaczmarek, P. Krüger, and T.M. Fromhold
(Dated: October 3, 2022)

We investigate smooth, low-noise, microtraps holding ultracold atoms at submicron distances from a two-dimensional electron gas (2DEG) carrying constant current. The trapped atoms are sensitive to ballistic transport effects in the 2DEG. Opening or closing a single conductance channel in a quantum point contact can, for example, split or merge Bose-Einstein condensates (BECs). In situ patterning of the ionized donor profile optimizes 2DEG-based conductors either for configurable microtrapping or for BEC microscopy of quantum electronic devices and transport in heterostructures and graphene.

PACS numbers: 37.10.Gh, 67.85.-d, 73.40.-c

Atom chips create microscopic potential landscapes for Bose-Einstein condensates (BECs) and degenerate Fermi gases [1, 2]. High sensitivity of ultracold atoms to changes in the trap potential has led to chip-based atom interferometry [3], field sensors [4, 5] and BEC microscopes [4, 6–8], which map current flow in classical metallic conductors with μm -scale resolution. Atom chips are also ideal for interfacing BECs with solid-state quantum systems such as superconducting wires [9]. Semiconductor heterostructures [10], or graphene [11], containing a two-dimensional electron gas (2DEG) form another major class of quantum electronic devices. Such systems exhibit rich fundamental physics – from the Quantum Hall Effects to single-photon sources and qubit manipulation – and have technological applications in resistance standards and high-mobility transistors for mobile communication [10]. Hybrid matter-wave devices with controlled quantum coupling between ultracold atoms and 2DEG-based circuits offer many possibilities [12], but depend critically on achieving submicron trapping distances.

In all experiments to date, atom-surface trapping distances exceed $1\ \mu\text{m}$. The common use of thick metal wires limits miniaturization of the potential landscape because of high Johnson noise in the wires [13–15] and strong atom-surface Casimir-Polder (CP) attraction [15]. In addition, imperfections in the wires produce spatial fluctuations in the trapping potential, thus modulating the density profile of a BEC [16–20]. Such fluctuations are undesirable from a trapping perspective and require oscillating rf currents to reduce them [17, 21].

In this paper, we show that 2DEG quantum electronic components fabricated in a GaAs/(AlGa)As heterojunction membrane [10, 22] overcome present limits on both the functionality and miniaturization of atom chips, thereby also broadening the scope of BEC microscopy [7]. Inhomogeneities in the 2DEG current produce spatial fluctuations in the density profile of a BEC held nearby. For a heterojunction, we find that the variation of the rms fluctuation amplitude, Δn^{rms} , with distance, z , from the 2DEG depends directly on, and so provides a *non-invasive* measurement of, the donor correlation function. This function is of fundamental importance for understanding and increasing 2DEG mobility [23–27], but cur-

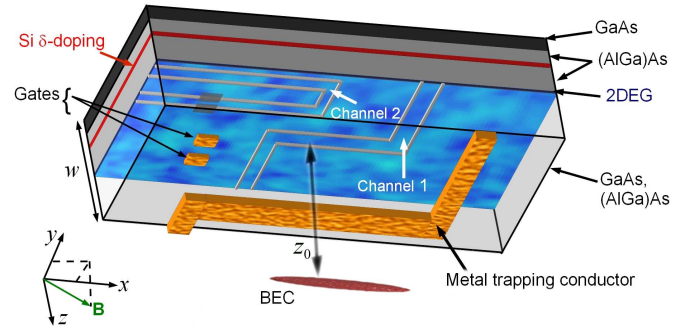


Figure 1: (Color) Schematic of a heterojunction-based atom chip comprising GaAs and (AlGa)As layers (labelled) in the $x - y$ plane (axes inset). Ionized Si donors (red layer) supply electrons to the 2DEG (blue), which lies in the $z = 0$ plane. GaAs and (AlGa)As layers below the 2DEG are shown semi-transparent for clarity. Insulating regions (gray) in the 2DEG enclose distinct conducting channels, 1 and 2. A BEC (red) is confined in a harmonic trap, centered in the $z = z_0$ plane, produced by an applied field, \mathbf{B} , (green arrow), and current through either the metal surface wire (yellow Z shape) or 2DEG Channel 1. Rectangular yellow regions are metal surface gates, which can be biased negatively to produce a QPC (dark gray shadow) in the lower arm of Channel 2.

rently hard to determine directly in experiment. When the ionized donors are distributed randomly, Δn^{rms} decreases more slowly with increasing z than for fabrication imperfections in metal wires [17, 28]. Consequently, the BEC density fluctuations are strong enough to detect the opening or closure of a single quantized conductance channel in a quantum point contact (QPC) [10, 27], which can split or re-merge the BEC. A single image of the BEC maps the current profile over hundreds of μm , providing single-shot functional imaging of quantum electronic devices and transport. In contrast to metal wires, the variation of Δn^{rms} with z can be controlled *in situ* by changing the distribution of ionized donors. Using optical illumination to pattern this distribution periodically makes the field fluctuations decay exponentially with increasing z so that Δn^{rms} is 3 orders of magnitude smaller than for a metal wire $\approx 1\ \mu\text{m}$ from the chip. This, com-

bined with low Johnson noise and weak CP attraction to membranes, makes 2DEGs – in heterojunctions or in graphene – ideal for producing smooth near-surface traps with long lifetimes, which are essential for creating hybrid cold-atom/quantum electronic systems.

We consider an atom chip built on a GaAs/(AlGa)As heterojunction, which traps a BEC near a 2DEG (Fig. 1). In the first part of the paper, the trapping potential is produced by current, I_w , through a Z-shaped metal surface wire (yellow in Fig. 1), combined with a uniform magnetic field $\mathbf{B} = (0, B_y, B_z)$, which positions the trap center at distance z_0 from conducting Channel 1 in the 2DEG [7]. The 2DEG is formed by electrons from ionized donors in a Si δ -doping layer (red in Fig. 1) [23, 25, 29], which migrate into the GaAs and populate the ground state of an almost triangular potential well formed at the GaAs/(AlGa)As interface [10, 25]. This confines the electrons in a narrow (≈ 15 nm thick) sheet (blue in Fig. 1). Insulating regions in the 2DEG (gray in Fig. 1), made by implanting Ga ions [30], enclose two distinct conduction channels, labelled 1 and 2 in Fig. 1.

Atom chips are usually built on a bulk substrate, which generates a strong CP attraction, thus preventing atoms being trapped closer than a few μm from the surface [15]. Recently, suspended trapping wires were used to reduce the CP potential [31]. Here, we consider a heterojunction membrane of width $w = 130$ nm, as in previous experiments [22]. For this structure, the CP potential energy, $V_{CP} \propto w/z^5$ ($z \gg w$) [32], is ten times smaller at $z = 1 \mu\text{m}$ than for a bulk semiconductor surface: weak enough to allow submicron trapping. Polarization of adsorbed atoms [33] can be minimized by surface passivation or judicious choice of surface reconstruction [12].

We take typical heterojunction parameters with $n_d = 3.3 \times 10^{15} \text{ m}^{-2}$ ionized donors at distance $d = 50$ nm from the 2DEG (Fig. 1) [12, 29, 34]. The 2DEG is 65 nm below the surface and of mean electron density equal to n_d . Since the 2DEG is so thin and ion implantation is accurate to $\approx 3\%$ of the channel width, surface and edge fluctuations are negligible: a major advantage over metal wires. We take the heterojunction temperature to be 4.2 K, as in superconducting atom chips [9], to ensure high 2DEG conductivity, $\sigma = 7.2 \times 10^{-2} \Omega^{-1}$, and that inhomogeneity in the current originates only from non-uniformity of the ionized donors [23, 25].

These donors create a spatially-varying attractive potential, which is partially screened by the 2DEG [10]. In the Thomas-Fermi screening model [34], the potential energy of a 2DEG electron at position $\mathbf{r} = (x, y)$ is

$$\Phi(\mathbf{r}) = \frac{e^2}{4\pi\epsilon\epsilon_0} \int e^{-kd} \frac{p_d(\mathbf{k}) e^{i\mathbf{k}\cdot\mathbf{r}}}{k + k_s} d^2\mathbf{k}, \quad (1)$$

where $\mathbf{k} = (k_x, k_y)$, $k = |\mathbf{k}|$, $p_d(\mathbf{k})$ is the 2D Fourier transform of the spatial ionized donor density, $p_d(\mathbf{r})$, ϵ is the relative permittivity of GaAs, and the screening wave vector, $k_s = e^2 m^* / (2\epsilon\epsilon_0 \pi \hbar^2)$, depends on the electron's charge magnitude, e , and effective mass, m^* [34].

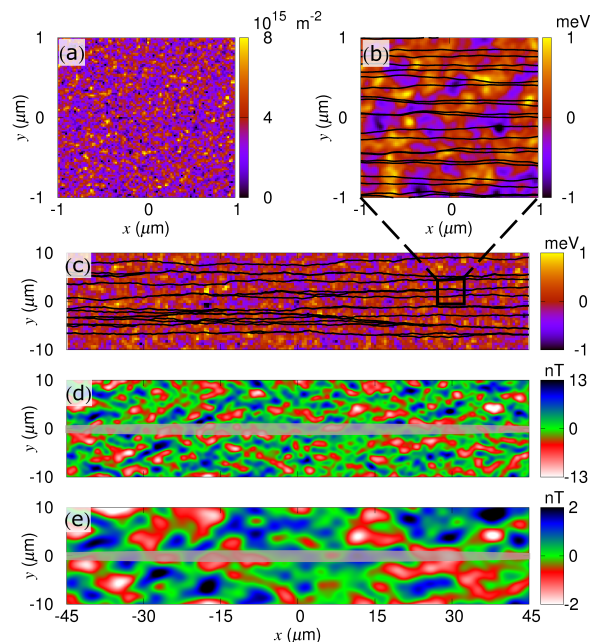


Figure 2: (Color) (a) Ionized donor density, $p_d(\mathbf{r})$, where $\mathbf{r} = (x, y)$. (b,c) Potential energy, $\Phi(\mathbf{r})$, in the 2DEG. Region enclosed by rectangle in (c) is enlarged in (b). (d,e) Magnetic field component $B_x(\mathbf{r}, z_0)$ at distance $z_0 =$ (d) $1 \mu\text{m}$, (e) $3 \mu\text{m}$ from the 2DEG. Black curves in (b,c) are current streamlines. Gray shapes in (d,e) mark the location of BEC A in the $z = z_0$ plane. Color bars to right of each panel show scales.

We now consider the electrostatic properties and current profile of Channel 1, of width $20 \mu\text{m}$ and central arm length $90 \mu\text{m}$. Figure 2 shows (a) a typical uncorrelated ionized donor distribution, $p_d(\mathbf{r})$, and (b,c) the screened potential energy in the 2DEG, $\Phi(\mathbf{r})$ [24].

When an applied voltage creates an electric field, \mathbf{E} , along Channel 1, the local current density is $\mathbf{j}(\mathbf{r}) = \sigma\mathbf{E} + \mathbf{j}_i(\mathbf{r})$, where the inhomogeneous component $\mathbf{j}_i(\mathbf{r}) = \sigma\nabla\Phi(\mathbf{r})/e$ originates from fluctuations in $p_d(\mathbf{r})$ and $\Phi(\mathbf{r})$.

The black curves in Fig. 2(b,c) show current streamlines calculated for $E = 10^4 \text{ Vm}^{-1}$. Inhomogeneity of $\Phi(\mathbf{r})$ makes these streamlines deviate from the x -direction. Consequently, the resulting magnetic field at position $\mathbf{r} = (x, y)$ in the $z = z_0$ plane has a non-zero x -component, given, from the Biot-Savart law [6], by

$$B_x(\mathbf{r}, z_0) = \frac{\mu_0 e \sigma}{4\epsilon\epsilon_0} \int \frac{k_y p_d(\mathbf{k})}{k + k_s} e^{-k(d+z_0)} e^{-i\mathbf{k}\cdot\mathbf{r}} d^2\mathbf{k} \quad (2)$$

Equation (2) reveals two key results. First, the fluctuations of $B_x(\mathbf{r}, z_0)$ depend directly on the donor distribution via $p_d(\mathbf{k})$. Second, due to the $e^{-k(d+z_0)}$ term, the field fluctuations become weaker and smoother as z_0 increases. This can be seen by comparing the color maps of $B_x(\mathbf{r}, z_0)$ in Fig. 2 for $z_0 =$ (d) $1 \mu\text{m}$ and (e) $3 \mu\text{m}$.

We now consider how the field fluctuations affect a BEC, henceforth called BEC A, comprising 10^4 ^{87}Rb atoms in state $|F = 2, m_F = 2\rangle$, whose position in the

$z = z_0$ plane is shown by the gray regions in Fig. 2(d,e). Since the BEC is strongly confined along y and z , its density profile is sensitive only to fluctuations in $B_x(\mathbf{r}, z_0)$. Along the x -axis [$\mathbf{r} = (x, 0)$], the atom density fluctuations are $\Delta n(x) = -(m_F g_F \mu_B / 2 \hbar \omega_r a_s) B_x(x, z_0)$ [7], where the g-factor $g_F = 1/2$, μ_B is the Bohr magneton and a_s is the s-wave scattering length. Consequently, measurements of $\Delta n(x)$ directly probe $B_x(x, z_0)$. By scanning the BEC over the 2DEG, such measurements can map $B_x(\mathbf{r}, z_0)$ above a large area of Channel 1 and be deconvoluted to determine $\mathbf{j}_i(\mathbf{r})$ [7, 8].

The variation of the oscillatory amplitudes of $\Delta n(x) \propto -B_x(x, z_0)$ with z_0 is crucial for understanding, and exploiting, the effect of 2DEG current on a BEC. To demonstrate this, we first calculate the rms average of $B_x(x, z_0)$ along x at fixed z_0 :

$$B_x^{rms}(z_0) = \left[\int B_x^2(x, z_0) dx \right]^{1/2} = \left(\frac{\mu_0 e \sigma}{4 \epsilon \epsilon_0} \right) \left[\int \int k_y k'_y \frac{S(\mathbf{k}, \mathbf{k}') e^{i k_x x + k'_x x'}}{(k + k_s)(k' + k_s)} \times e^{-(k+k')(d+z_0)} d^2 \mathbf{k} d^2 \mathbf{k}' \right]^{1/2} \quad (3)$$

Equation (3) reveals that $B_x^{rms}(z_0)$ depends directly on the correlation function, $S(\mathbf{k}, \mathbf{k}') = \langle p_d(\mathbf{k}) p_d(\mathbf{k}') \rangle$, of the ionized donor distribution in \mathbf{k} -space. BEC microscopy [7, 8, 17] can determine $B_x^{rms}(z_0)$ and so provide a *non-invasive* measurement of the donor correlation function. Donor statistics are of fundamental importance to electron transport and mobility [23–27], but usually inferred from theoretical models due to a lack of non-invasive experimental probes [25, 27]. X-ray scattering techniques have detected individual donor clusters [26]. But BEC microscopy [7, 8, 17] can probe the donor correlation function over a far wider range of length scales. Although the correlation function can be extracted from $B_x^{rms}(z_0)$ alone, BEC microscopy measures the full spatial profile of the magnetic field [6–8], and may therefore yield additional information about the donor distribution.

For a random donor distribution (Fig. 3 right inset) [24], $S(\mathbf{k}, \mathbf{k}') \propto \delta(\mathbf{k} + \mathbf{k}')$. Using this in Eq. (3) gives $B_x^{rms}(z_0) \sim 1/z_0^2$ (solid curve in Fig. 3), meaning that field fluctuations decay more slowly above a 2DEG than the $B_x^{rms}(z_0) \sim 1/z_0^{2.5}$ variation (dot-dashed curve in Fig. 3) known for metal wires [28]. As a result, BEC microscopy can measure $B_x^{rms}(z_0)$ over a wide range of z_0 , with an upper limit where the density fluctuations become too small to detect ($\lesssim 10\%$ of the unperturbed atom density [8]), and a lower limit set by the minimum BEC-surface separation. Trapping the BEC $< 1 \mu\text{m}$ from the surface provides sufficient resolution to image, *in situ* and over a large area, the complex electron redistribution that occurs during metal-insulator transitions in a 2DEG [25, 35], in quantum dots and, possibly, during QPC switching at the 0.7 conduction anomaly [10].

The ionized donor distribution, and hence the form of $B_x^{rms}(z_0)$, can be controlled by illuminating the hetero-

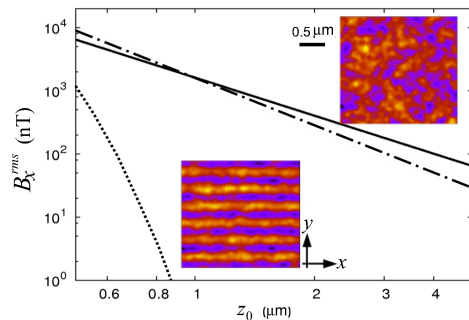


Figure 3: (Color) $B_x^{rms}(z_0)$ above Channel 1 calculated for spatially random (solid curve) and periodically-modulated (dotted curve) ionized donor profiles in x - y plane (right- and left-hand insets respectively: horizontal bar is spatial scale). For comparison, the dot-dashed curve shows $B_x^{rms}(z_0) \sim 1/z_0^{2.5}$ characteristic of a metal wire [28].

junction [26]. Since the number of ionized donors increases with the local light intensity, two laser beams counter-propagating along y , each of wavelength λ , spatially modulates the donor distribution with a period $\lambda_y = \lambda/2$ (Fig. 3 left inset). In this case, $S(\mathbf{k}, \mathbf{k}') \propto [\delta(k + k_0)\delta(k' - k_0) + \delta(k - k_0)\delta(k' + k_0)]$, where $k_0 = 2\pi/\lambda_y$. Using this in Eq. (3) gives $B_x^{rms}(z_0) \sim \exp(-z_0/\lambda_y)$, shown for $\lambda = 660 \text{ nm}$ by the dotted curve in Fig. 3. This rapid decay occurs because, as in a magnetic mirror, the current streamlines align with the striped donor distribution (Fig. 3 left inset), which reduces meandering of the current and, hence, the field fluctuations.

The ability to tailor the transport properties of the 2DEG, and the resulting field fluctuations, is a unique feature of heterojunctions, which can be exploited for trapping, manipulating, and imaging with, ultracold Bose gases. Crucially, exponential decay makes the $B_x^{rms}(z_0)$ curve for the periodically-modulated donor distribution (dotted in Fig. 3) fall rapidly below that for a metal wire (dot-dashed curve in Fig. 3). At $z_0 \gtrsim 0.8 \mu\text{m}$, the field fluctuations above the 2DEG are more than 3 orders of magnitude smaller than for the metal wire.

Consequently, 2DEGs have great potential for creating high-quality near-surface microtraps. To demonstrate this, we consider the trap produced by a 0.8 mA current through 2DEG Channel 1 *only* (Fig. 1), setting $I_w = 0$. The solid curve in Fig. 4(a) shows the total potential energy $V_{tot}(z) = V_m(z) + V_{CP}(z)$ calculated for a ^{23}Na atom, where $V_m(z)$ originates from the magnetic field produced by Channel 1 and an applied field $\mathbf{B} = (40, 57, 0) \text{ mG}$. Since the CP attraction is weak, the trap is deep enough to confine BEC B , comprising 500 ^{23}Na atoms in state $|F = 1, m_F = -1\rangle$, whose chemical potential [horizontal line in Fig. 4(a)] is far below the top of the left-hand barrier. Even though the trap center is only $0.7 \mu\text{m}$ from the 2DEG [Fig. 4(a)], V_{tot} varies very smoothly with x [solid curve in Fig. 4(b)] because $B_x^{rms}(z_0)$ is only $\approx 20 \text{ nT}$ (Fig. 3). Even at 4.2 K, the resistance of Channel 1 is ≈ 10 times higher than a

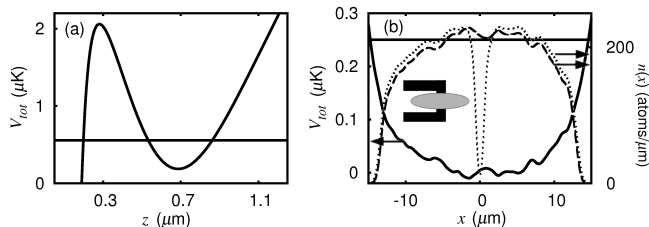


Figure 4: (a,b): V_{tot} (solid curve) for a ^{23}Na atom versus (a) z , (b) x at $z_0 = 0.7 \mu\text{m}$ above the center of Channel 1 (Fig. 1). Horizontal lines in (a,b): chemical potential of BEC B in the trap. In (b), dashed (dotted) curve shows for $N = 0$ (1) the density of BEC B , $n(x)$, along the trap center, which is displaced so that the BEC (schematic gray shape in inset) lies above the central arm (black in inset) of Channel 2.

similarly-sized gold conductor at room temperature [36]. Consequently, 2DEGs offer lower Johnson noise and resulting spin-flip loss rates than metal wires. Like superconducting traps [9], the lifetime of atoms in 2DEG traps would primarily be limited by collisions with background atoms or three body losses.

Near-surface trapping makes the BEC highly sensitive to magnetic field variations arising from the *geometry* of the conduction channels, such as local narrowing. As an example, suppose that \mathbf{B} is adjusted to hold BEC B across the middle arm of U-shaped Channel 2 [Figs. 1 and 4(b) inset]. Channel 2 is narrow enough (20 nm) for the electrons to populate a small number, N , of discrete energy levels, E_l ($l = 0, 1, 2, \dots, N$), corresponding to motion across it. Along the channel, whose quantized conductance is $G = 2Ne^2/h$ [10, 26], electrons occupy one-dimensional plane wave states up to the Fermi level. Applying a negative voltage, $-|V_g|$, to metal surface gates (yellow rectangles in Fig. 1), which are on either side of the lower arm of Channel 2 and sufficiently far from the BEC to have negligible electrostatic effect on it, locally depletes the 2DEG. This narrows the con-

duction channel, forming a QPC and raising E_l . As V_g increases, the energy levels pass successively through the Fermi level and depopulate [10, 26, 27]. Depopulation of each level abruptly decreases N and, consequently, the current through Channel 2 by $\Delta I = 2e^2V/h$, where V is the voltage dropped across the QPC.

The dashed curve in Fig. 4(b) shows the density profile, $n(x)$, of BEC B when the QPC in Channel 2 is fully depleted ($N = 0$). Since the QPC carries no current in this case, $n(x)$ is the unperturbed ground state of the trapping potential shown by the solid curves in Fig. 4(a,b). Opening a *single* conduction channel in the QPC ($N = 1$) changes the trap profile sufficiently to almost completely split the BEC [dotted curve in Fig. 4(b)]. Consequently, the BEC can detect quantized changes in the QPC's conductance, which, conversely, can manipulate the BEC, for example splitting and recombining it in atom interferometry. More complex shaping of the atom cloud is also possible: an array of QPCs could imprint and control a wide range of sub- μm patterns in the BEC.

In summary, ballistic electron transport in heterojunctions can create smooth, low-noise, magnetic traps, which provide the sub- μm control required to integrate ultracold atoms with quantum electronic systems. By tailoring the donor distribution, magnetic field fluctuations can be suppressed exponentially without recourse to rf signals and wires, leaving the chip surface free for components such as voltage gates. Quantum transport processes in a 2DEG can imprint strong density modulations in a BEC, which, conversely, provide a non-invasive probe of those processes. The ability to measure the potential landscape and mobility of a 2DEG *independently* may yield new insights for understanding how the two relate and, hence, for increasing 2DEG mobility [37, 38]. Suspended graphene membranes, which combine low CP attraction with very high room-temperature carrier mobility [11], could be the ultimate material for sub- μm atom trapping and BEC microscopy of quantum transport [39].

-
- [1] For reviews see: J. Reichel, Appl. Phys. B: Lasers Opt. **74**, 469 (2002); R. Folman *et al.*, Adv. At. Mol. Opt. Phys. **48**, 263 (2002); J. Fortágh and C. Zimmermann, Rev. Mod. Phys. **79**, 235 (2007).
- [2] S. Aubin, S. Myrskog, M. H. T. Extavour, L. J. LeBlanc, D. McKay, A. Stummer, and J. H. Thywissen, Nature Physics **2**, 384 (2006).
- [3] T. Schumm *et al.* Nature Physics **1**, 57 (2005); G.-B. Jo *et al.*, Phys. Rev. Lett. **98**, 180401 (2007).
- [4] B. V. Hall, S. Whitlock, R. Anderson, P. Hannaford, and A. Sidorov, Phys. Rev. Lett. **98**, 030402 (2007).
- [5] Some magnetic sensors use optical traps: M. Vengalattore, J.M. Higbie, S.R. Leslie, J. Guzman, L.E. Sadler, and D.M. Stamper-Kurn, Phys. Rev. Lett. **97**, 200801 (2007).
- [6] B. Roth, N. Sepulveda, and J. Wikswo, J. Appl. Phys. **65**, 361 (1989).
- [7] S. Wildermuth *et al.*, Nature **435**, 440 (2005); Appl. Phys. Lett. **88**, 264103 (2006).
- [8] S. Aigner, L. D. Pietra, Y. Japha, O. Entin-Wohlman, T. David, R. Salem, R. Folman, and J. Schmiedmayer, Science **319**, 1226 (2008).
- [9] T. Mukai *et al.*, Phys. Rev. Lett. **98**, 260407 (2007); C. Roux *et al.*, Eur. Phys. Lett. **81**, 56004 (2008).
- [10] K.-F. Berggren and M. Pepper, Phil. Trans. R. Soc. A **368**, 1141 (2010), and Refs. therein.
- [11] A. K. Geim, Science **324**, 1530 (2009).
- [12] T. E. Judd, R. G. Scott, G. Sinuco, T. W. A. Montgomery, A. M. Martin, P. Krüger, and T. M. Fromhold, New J. Phys. **12**, 063033 (2010).
- [13] C. Henkel, Eur. Phys. J. D **35**, 59 (2005).
- [14] C. D. J. Sinclair, E. A. Curtis, I. L. Garcia, J. A. Retter, B. V. Hall, S. Eriksson, B. E. Sauer, and E. A. Hinds, Phys. Rev. A **72**, 031603(R) (2005).

- [15] Y. Lin, I. Teper, C. Chin, and V. Vuletić, *Phys. Rev. Lett.* **92**, 050404 (2004).
- [16] D.-W. Wang, M. D. Lukin, and E. Demler, *Phys. Rev. Lett.* **92**, 076802 (2004).
- [17] P. Krüger, L. M. Andersson, S. Wildermuth, S. Hofferberth, E. Haller, S. Aigner, S. Groth, I. Bar-Joseph, and J. Schmiedmayer, *Phys. Rev. A* **76**, 063621 (2007).
- [18] J. Fortágh, H. Ott, S. Kraft, A. Günther, and C. Zimmermann, *Phys. Rev. A* **66**, 041604 (2002).
- [19] M. P. A. Jones, C. J. Vale, D. Sahagun, B. V. Hall, and E. A. Hinds, *Phys. Rev. Lett.* **91**, 080401 (2003).
- [20] J. Estève, C. Aussibal, T. Schumm, C. Figl, D. Maily, I. Bouchoule, C. I. Westbrook, and A. Aspect, *Phys. Rev. A* **70**, 043629 (2004).
- [21] J. B. Trebbia, C. L. G. Alzar, R. Cornelussen, C. I. Westbrook, and I. Bouchoule, *Phys. Rev. Lett.* **98**, 263201 (2007).
- [22] R. H. Blick, F. G. Monzon, W. Wegscheider, M. Bichler, F. Stern, and M. L. Roukes, *Phys. Rev. B* **62**, 17103 (2000); E. M. Höhberger, T. Krämer, W. Wegscheider, and R. H. Blick, *Appl. Phys. Lett.* **82**, 4160 (2003).
- [23] E. Buks, M. Heiblum, and H. Shtrikman, *Phys. Rev. B* **49**, 14790 (1994).
- [24] P. T. Coleridge, *Semicond. Sci. Technol.* **12**, 22 (1997).
- [25] R. Grill and G. H. Döhler, *Phys. Rev. B* **59**, 10769 (1999).
- [26] J. J. Koonen, H. Buhmann, and L. W. Molenkamp, *Phys. Rev. Lett.* **84**, 2473 (2000).
- [27] M. A. Topinka, B. J. LeRoy, R. M. Westervelt, S. E. J. Shaw, R. Fleischmann, E. J. Heller, K. D. Maranowski, and A. C. Gossard, *Nature* **410**, 183 (2001).
- [28] T. Schumm, J. Estève, C. Figl, J.-B. Trebbia, C. Aussibal, H. Nguyen, D. Maily, I. Bouchoule, C. I. Westbrook, and A. Aspect, *Eur. Phys. J. D* **32**, 171 (2005).
- [29] Additional doping layers (not shown in Fig. 1) supply electrons to surface states [12].
- [30] K. Ensslin and P. M. Petroff, *Phys. Rev. B* **41**, 12307 (1990).
- [31] H.-C. Chuang, E.A. Salim, V. Vuletić, D.Z. Anderson, and V.M. Bright, *Sensors and Actuators A: Physical*, in press (2010).
- [32] A. M. Contreras Reyes and C. Eberlein, *Phys. Rev. A* **80**, 032901 (2009).
- [33] D. Hunger, S. Camerer, T. W. Hänsch, D. König, J. P. Kotthaus, J. Reichel, and P. Treutlein, *Phys. Rev. Lett.* **104**, 143002 (2010).
- [34] A. L. Efros, F. G. Pikus, and V. G. Burnett, *Phys. Rev. B* **47**, 2233 (1993).
- [35] S. Ilani, A. Yacoby, D. Mahalu, and H. Shtrikman, *Science* **292**, 1354 (2001).
- [36] R. Salem, Y. Japha, J. Chabé, B. Hadad, M. Keil, K. A. Milton, and R. Folman, *New J. Phys.* **12**, 023039 (2010).
- [37] S. J. MacLeod, K. Chan, T. P. Martin, A. R. Hamilton, A. See, A. P. Micolich, M. Aagesen, and P. E. Lindelof, *Phys. Rev. B* **80**, 035310 (2009).
- [38] V. Umansky, M. Heiblum, Y. Levinson, J. Smet, J. Nübler, and M. Dolev, *J. Crystal Growth* **311**, 1658 (2009).
- [39] We predict traps $\approx 10 \mu\text{K}$ deep $\approx 600 \text{ nm}$ from room-temperature graphene.